Influence of Confinement on Barriers for Alkoxide Formation in Acidic Zeolites

Michal Fečík,[a] Philipp N. Plessow,*[a] and Felix Studt*[a, b]

The influence of the confinement imposed by eight different zeotypes on the formation of the alkoxides of 13 primary alcohols is studied using dispersion corrected density functional theory calculations with the PBE-D3 functional. Adsorption energies of the alcohols are computed along with barriers for formation of the alkoxides, which is the first step of the stepwise dehydration mechanism. We find that variations in the adsorption and transition state energies are largely governed by van der Waals interactions between substrates and the zeolite framework. Trends between different reactants, on the other hand, are largely due to the size of the molecules, which can be described quantitatively by the number of atoms constituting them. We find that the stabilization of adsorbates is largest for frameworks that are neither too small, leading to repulsive interaction, nor too spacious leading only to weak interaction.

Introduction

Motivated by the performance of enzymes in highly selective bio-catalytic conversions that is associated to their specific steric environment, there is vivid interest in advancing our understanding of the effects of confinement in homo- and heterogeneous catalysis.[1–2] Perhaps the best example in the field of heterogeneous catalysis is given by zeolites, that provide a microscopic pore structure within which the reaction occurs. Due to this specific chemical environment, the catalyzed reactions are often highly selective. Catalysis by zeolites is experiencing renewed interest and growth as zeolites are thought to become the catalysts of choice for future processes such as the methanol-to-hydrocarbon or olefins processes[3–6] and the tailored conversion of biomass derived feedstocks.[7–8]

The high potential of zeolites is attributed to their performance for important acid-catalyzed reactions, such as the conversion of fructose to 5-HMF[9–10] and glycerol to acrolein.[11–15] A detailed understanding of how the effect of confinement influences the activity and selectivity of dehydration reactions related to these conversions is therefore highly desirable. Density functional theory (DFT) calculations offer a useful tool to investigate the reaction mechanisms and the intrinsic effect of the confinement in great detail[16–22] and to deduct trends from one material to another.[23–26]

DFT calculations also help understanding, how electronic and steric effects influence reaction barriers and adsorption energies within zeolite pores. Taking the dehydration of a range of alcohols in H-ZSM-5 (MFI framework) as an example, we recently showed how reaction barriers relate to the interaction between the adsorbate and the zeolite through dispersion forces.[19] Furthermore, we were able to invoke a simple scheme based on a straightforward measure of dispersion forces that allowed to predict transition state energies of dehydration reactions quite accurately. Herein, we investigate how the acid catalyzed dehydration of alcohols within a variety of microporous zeotypes depends on the confinement imposed by the porous framework. In the present study, we investigate the primary alcohols shown in Scheme 1b and the according first step of their dehydration (Scheme 1a) over 6 different zeolite frameworks, where we focus on one T-site for Al-substitution in each case. We note that the reactivity of T-sites differ to some extent, e.g. when probing the 12 different T-sites using the ammonia heat of adsorption, reactivity was found to vary by 29 to 39 kJ/mol.[27]

Herein, we focus on alkoxide formation as the first step of the stepwise dehydration as it was shown to be typically the rate-determining step,[28,29] while the second step, leading either to ether or olefin formation typically requires a lower barrier.[15,30–34] We note that dehydration can also occur via the concerted mechanism, which is typically favored at lower temperatures.[28,29] The studied frameworks, already including the Brønsted acid site, with their corresponding pore diameters (and diameters of pore openings when present) are shown in Figure 1.

[a] M. Fečík, Dr. P. N. Plessow, Prof. F. Studt
Institute of Catalysis Research and Technology
Karlsruhe Institute of Technology
Hermann-von-Helmholtz Platz 1
76344 Eggenstein-Leopoldshafen (Germany)
E-mail: philipp.plessow@kit.edu
[b] Prof. F. Studt
Institute of Chemical Technology and Polymer Chemistry
Karlsruhe Institute of Technology
Engessestrasse 18
76131 Karlsruhe (Germany)
E-mail: felix.studt@kit.edu

Supporting information for this article is available on the WWW under https://doi.org/10.1002/cctc.202100009

This publication is part of a Special Collection on "Catalysis in Confined Spaces". Please check the ChemCatChem homepage for more articles in the collection.

a)

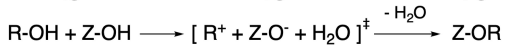

b)

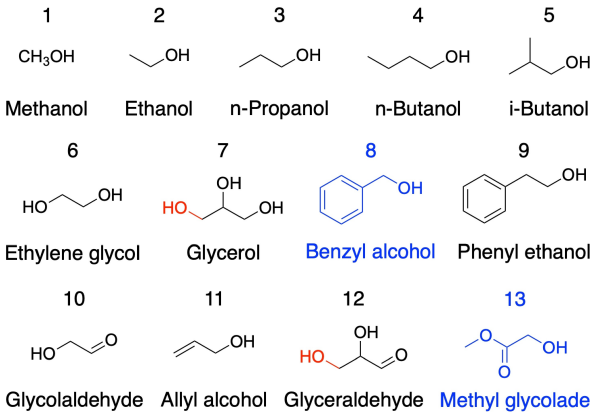

Scheme 1. (a) Studied reaction mechanism with R standing for an alcohol group. IS, TS and FS are initial, transition and final states respectively. **(b)** Investigated reactants. The dehydrated hydroxy group is shown in red for the cases where multiple possibilities exist. Reactants exhibiting strong mesomeric effects are highlighted in blue.

Results and Discussion

We start by comparing the energetics of the formation of a surface methoxy species (SMS) from methanol (MeOH) in the various zeolites. This reaction starts with the adsorption of MeOH, constituting the initial state (IS), through a hydrogen bond between the acid site and methanol. Methanol is then protonated and the methyl group is transferred to the negatively charged zeolite and water is released. As mentioned in our previous work for SMS formation in H-SZM-5,[19] and in a study by Hibbitts and coworkers for SMS-formation with co-adsorbed toluene,[35] the barriers for protonation/rotation of the alcohols are negligible compared to the barrier for methylation. This reaction has been investigated theoretically to a great extend[30,36–41] as it constitutes the first step in stepwise (or dissociative) methylation reactions (e.g. stepwise formation of dimethyl ether (DME) via MeOH). We computed the adsorption energy of MeOH for various frameworks and obtained binding energies ranging from −91 kJ/mol (H-SAPO-34) to −119 kJ/mol (H-MOR and H-ZSM-22, see Table 1) in good agreement with earlier theoretical studies (see Table S4 for an in-depth comparison with data available in the literature).[36–41] The reaction of adsorbed MeOH with the acid site forming an SMS and water is computed to have reaction barriers ranging from 126 kJ/mol (H-SAPO-34) to 150 kJ/mol (H-BEA) when referenced to the adsorbed MeOH.

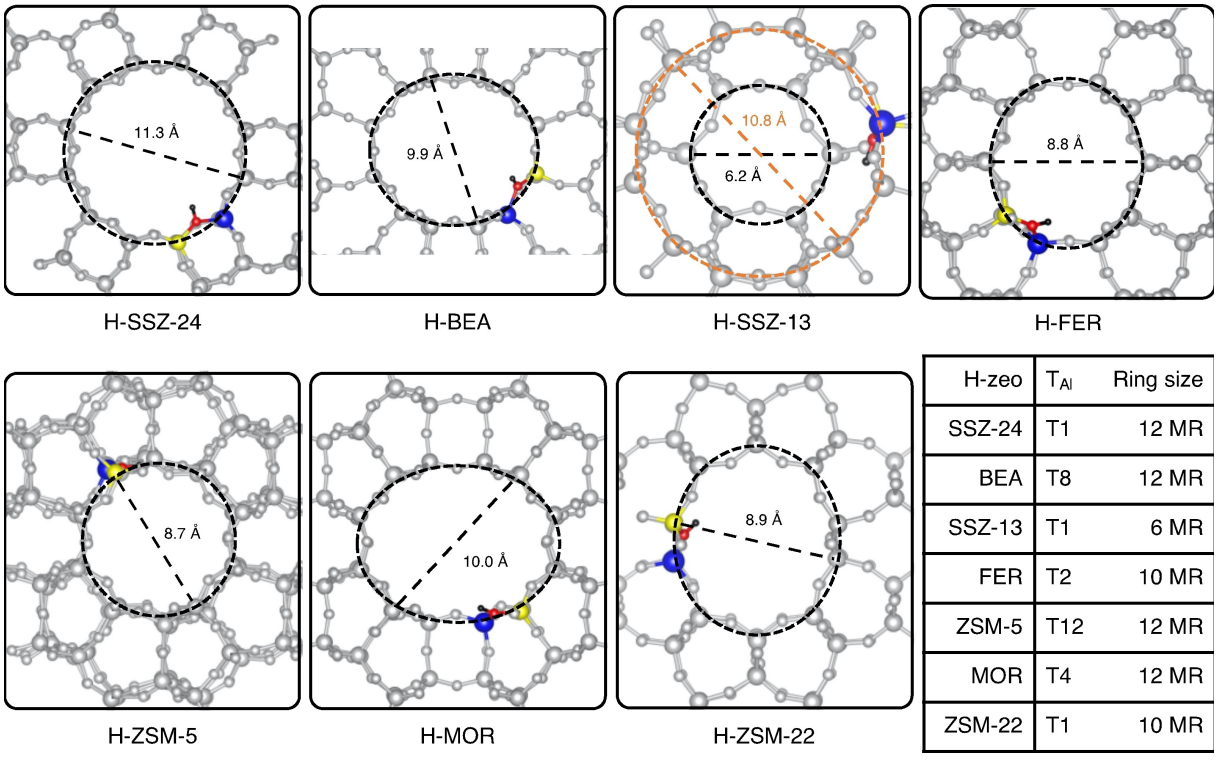

H-zeo	T_{Al}	Ring size
SSZ-24	T1	12 MR
BEA	T8	12 MR
SSZ-13	T1	6 MR
FER	T2	10 MR
ZSM-5	T12	12 MR
MOR	T4	12 MR
ZSM-22	T1	10 MR

Figure 1. The pore structures of the studied zeolites where the shortest Si-Si distance(s) is shown together with the highlighted pore structure (dashed circle/ellipse). The shown diameters do not include van der Waals radii. In case of H-SSZ-13, the diameter of the pore opening (black) is shown together with effective cavity diameter (orange). H-SAPO-34 has the same framework as H-SSZ-13, and thus is not explicitly shown. Tetrahedra atoms chosen for Al substitution (T_{Al}) and ring sizes highlighted by the black dashed line are shown in the legend – the ring sizes are given in number of members constituting the according rings (x MR = x-membered ring). Atoms at the active site are colored as Si = yellow, O = red, Al = blue, H = black, while the remaining framework atoms are shown in gray.

Table 1. Overview of the computed initial state (IS), transition state (TS) and intrinsic activation (TS-IS) energies for all studied reactants and all considered zeolite frameworks. All energies are in kJ/mol, ZPVE corrected and referenced to the empty zeotype and corresponding oxygenate in the gas-phase.

	energies [kJ/mol]												
zeolite	1	2	3	4	5	6	7	8	9	10	11	12	13
IS													
H-SSZ-24	−101	−113	−127	−137	−142	−122	−147	−164	−167	−104	−126	−126	−121
H-BEA	−107	−113	−136	−143	−145	−129	−154	−157	−166	−101	−122	−141	−119
H-SSZ-13	−113	−132	−139	−154	−137	−132	−173	−173	−155	−109	−129	−139	−138
H-FER	−116	−131	−147	−152	−158	−145	−156	−183	−179	−120	−141	−145	−134
H-ZSM-5[a]	−115	−132	−145	−159	−152	−125	−156	−164	−188	−114	−131	−147	−129
H-MOR	−119	−115	−143	−139	−139	−121	−142	−178	−164	−94	−114	−130	−124
H-SAPO-34	−91	−120	−128	−144	−128	−123	−157	−166	−149	−103	−122	−131	−133
H-ZSM-22	−119	−139	−150	−153	−141	−134	−169	−180	−183	−117	−141	−136	−134
TS													
H-SSZ-24	47	25	4	−6	4	14	−6	−58	−34	40	−12	17	39
H-BEA	43	16	8	−6	19	20	−14	−62	−30	44	−10	9	45
H-SSZ-13	21	2	−12	−29	−2	23	−12	−51	−43	25	−19	−5	27
H-FER	31	9	2	−1	14	21	−6	−13	−20	26	−20	41	47
H-ZSM-5[a]	25	12	−13	−29	−8	2	−23	−84	−49	27	−20	3	31
H-MOR	22	9	−2	−6	−5	7	−6	−57	−25	32	−10	27	34
H-SAPO-34	35	19	5	−9	13	32	5	−54	−30	36	0	6	37
H-ZSM-22	27	1	−17	−35	−6	6	−22	−88	−25	22	−31	4	30
TS-IS													
H-SSZ-24	148	138	131	131	146	136	141	106	133	144	114	143	160
H-BEA	150	129	144	137	164	149	140	95	136	145	112	150	164
H-SSZ-13	134	134	127	125	135	155	161	122	112	134	110	134	165
H-FER	147	140	149	151	172	166	150	170	159	146	121	186	181
H-ZSM-5	141	145	132	130	144	127	133	80	139	141	111	150	160
H-MOR	141	124	141	133	134	128	136	121	139	126	104	157	158
H-SAPO-34	126	139	133	135	141	155	162	112	119	139	122	137	170
H-ZSM-22	146	140	133	118	135	140	147	92	158	139	110	140	164

[a] Taken from Ref. [19].

We calculated the analogous reaction of ethanol (EtOH) with the acid site producing a surface ethoxy species (SES) for the eight acidic zeotypes considered herein as shown in Figure 2. In each case, we focus on the reactivity of one specific choice of T-site, where we choose positions that have been investigated previously.[19,42–51] Similar to the MeOH case, we obtain adsorption energies of EtOH ranging from −113 kJ/mol (H-SSZ-24 and H-BEA) to −139 kJ/mol (H-ZSM-22) (see also Table 1). Compared to the SMS formation from methanol, the SES formation is on average about 14 kJ/mol lower in energy which is in good agreement with an earlier study for H-ZSM-5.[19] Likewise, the transition state (TS) for SES formation has been calculated to range from 124 kJ/mol (H-MOR) to 144 kJ/mol (H-FER), when referenced to adsorbed EtOH. The final state (FS) is also lower by 14 kJ/mol on average. Note, that the final state energy is given for the alkoxide and desorbed water in the gas phase. We use this reference rather than co-adsorbed water in the final state, because water desorption becomes favorable at higher temperatures due to entropic effects. In earlier work employing H-ZSM-5, we identified a difference between MeOH and EtOH of 17, 13, and 18 kJ/mol for the IS, TS and FS, respectively.[19] Similar differences are also observed for the other seven zeotypes as shown in Figure 3, where the transition states of SMS and SES formation are compared. On average SES formation has 20 kJ/mol lower barriers compared to SMS formation, when referenced to the corresponding gas-phase oxygenate, as shown in Figure 3. Our earlier study explained these differences, e.g. observed between MeOH and EtOH, as being due to differences in dispersion interactions of the substrates with the pore of H-ZSM-5, rather than to changes in the interaction between the acid site and the substrates.[19] Given that this trend is observed across all eight zeotypes investigated here, this seems to be a general observation, that we will explore in the following.

Figure 3 shows a comparison between the transition state energy of the SMS and SES formation for all 8 zeotypes considered herein relative to methanol and ethanol in the gas-phase, respectively.

Apart from methanol and ethanol, we considered 11 other alcohols (shown in Scheme 1b) with relevance to biomass conversion. We calculated the transition state energy for the formation of the corresponding alkoxides and a comparison, analogous to that performed in Figure 3, is given in the supporting information, see Section S5 of the SI. Generally, we find a similar behavior to that shown in Figure 3, namely that there is a correlation between the transition state energies of the various alcohols considered herein.

In our earlier work,[19] we showed that this difference in transition state energies is mainly due to differences in the dispersion forces between the zeolite (in this case H-ZSM-5) and the corresponding alcohol, as long as the alcohol is not subject to strong repulsive interaction with the zeolite pore or

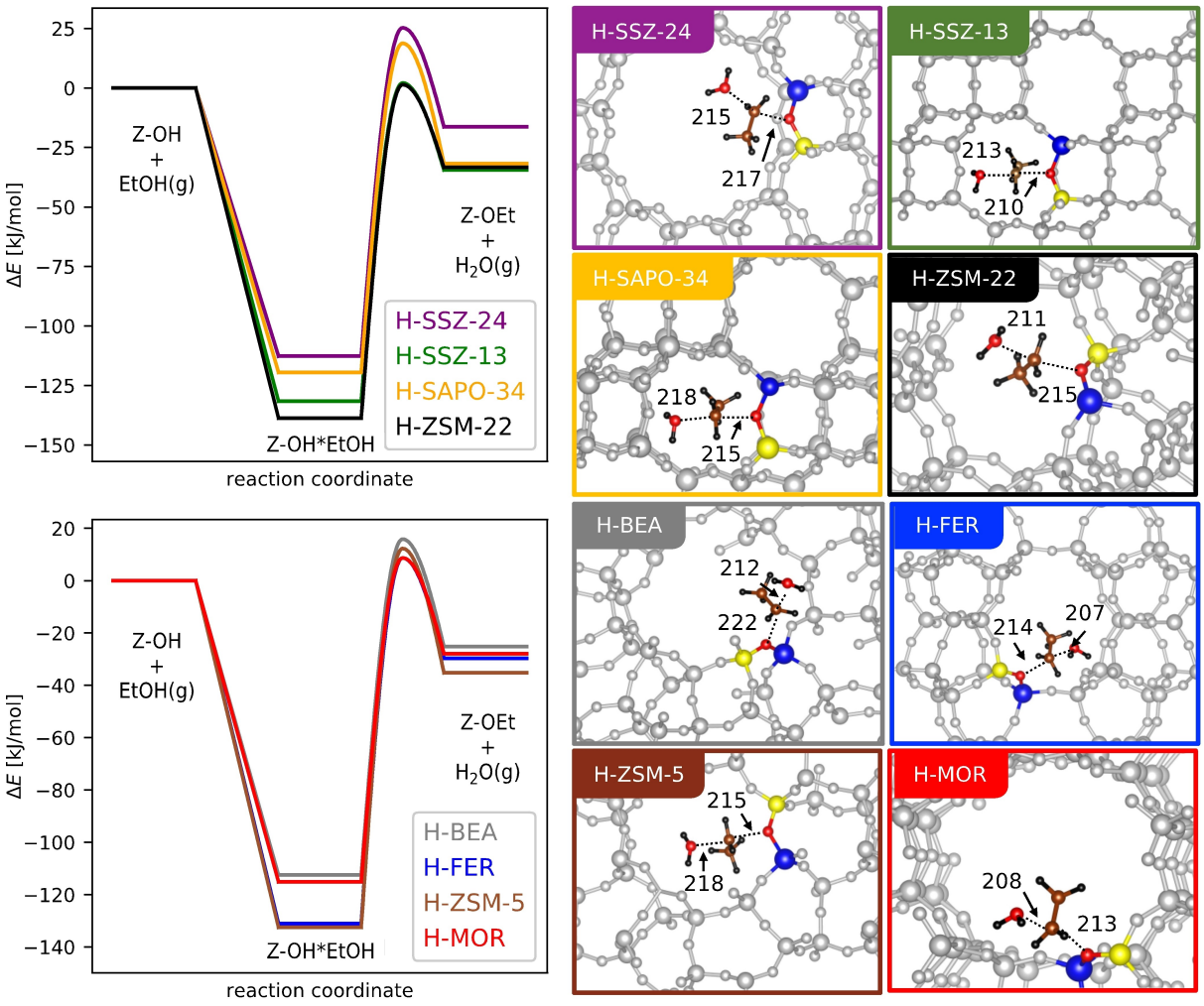

Figure 2. Energy diagrams of the formation of SES from ethanol (EtOH) for all the studied zeolite frameworks (left) together with shown corresponding transition state geometries in each of these cases. All energies are referenced to gas phase ethanol and the empty zeolite. All energies are given in kJ/mol and are corrected for zero-point vibrational energy (ZPVE) contributions. The initial states are EtOH adsorbed on the acid site, while the final state is the SES with desorbed water in the gas-phase.

stabilized due to mesomeric effects. We therefore computed the dispersion forces (the D3 part of the values obtained with the PBE-D3 functional) of the transition state energies for the various alcohol – zeotype configurations (see Figure 4).

Figure 4 shows that the van der Waals (vdW) contributions scale linearly with the total number of atoms of reactants inside zeolite pores with inclusion of the Brønsted proton. It is easily observed that each single zeolite framework scales with a different slope which is to be expected due to different sizes of the corresponding pores. Numerical values of these respective slopes are shown in Table S3 in the SI together with their correlations to the accessible volume of each zeolite framework and the maximum diameter of a sphere that can be included within them. It becomes also clear that there are two reactants that tend to be systematically more stable than the trend would suggest. These two reactants are benzyl alcohol (N = 17) and phenyl ethanol (N = 20) (represented by squares in Figure 4), i.e. the only aromatic reactants considered herein. We also find in some cases significant difference in between the vdW contribution between IS and TS. This may to some extent be due to the different orientation of the alcohols, as shown in Figure S18.

The computed initial and transition state energies are also illustrated in Figure 5. One can clearly observe trends in terms of the substrate, for example the mentioned aromatic reactants (8 and 9) have particularly low initial and transition state energies. As in previous work,[19] we find that the transition state energy decreases systematically when going from MeOH, over EtOH and propanol to butanol. This can be attributed to the increase in vdW interaction as shown in Figure 4. We find relatively high transition state energies for the glyceraldehyde, glycolaldehyde and methyl glycolate molecules, which we attribute to unfavorable, electron withdrawing mesomeric effects.

For the trends of the different investigated catalysts, the main observation is that H-SAPO-34 typically leads to high transition state energies. This can be, at least partially, explained by the lower acidity of H-SAPO-34 compared to the other

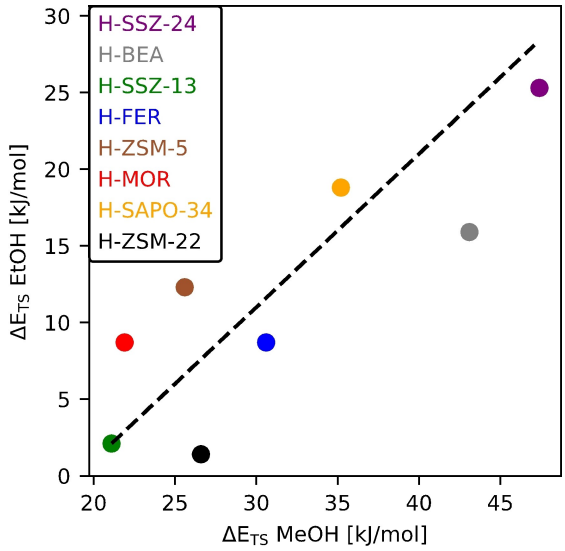

Figure 3. Comparison of the transition state energies (ΔE_{TS}) for the conversion of EtOH to SES and MeOH to SMS for the eight studied zeotypes. All energies are relative to the corresponding alcohol in the gas-phase and the acid site without adsorbants. The dashed line has a slope of 1 and the offset ($\Delta E = 21$ kJ/mol) corresponds to energy of the transition state of MeOH for H-SSZ-13) has been fitted through the data point for H-SSZ-13. All energies are in kJ/mol and ZPVE corrected. The mean absolute error (MAE) with respect to the dashed line is 4.3 kJ/mol.

zeotypes. Similarly, the strongest adsorption of the studied alcohols can be identified mainly for H-SSZ-13, H-FER, H-ZSM-5 and H-ZSM-22. The same tends to be true also for the lowest TS energies with the exception of H-FER. In terms of the confinement effect imposed by the zeotypes, the most obvious effect is the destabilization of the transition state involving the bulky aromatic molecules 8 and 9 in the small pore zeolite ferrierite. The zeolites H-BEA and H-SSZ-24 generally lead to weak vdW interaction (Figure 4) and the overall transition state and initial state energies shown in Figure 5 are also generally among the weakest. This is also apparent in Brønsted-Evans-Polanyi (BEP) relations shown in Figure S34a, where E_{TS} is shown as a function of E_{IS}. Intrinsic activation barriers (E_{TS}-E_{IS}) are analyzed in Table 1 and Figure S32. We find that the variation in intrinsic barriers is typically smaller than in the initial state and transition state energies and no clear trend is found in BEP relations shown in Figure S34b. This is because variations of initial state and transition state energies between the zeolites are similar in nature such that these trends partially cancel out. In terms of intrinsic activation barriers, most reactants are in a similar range of 125 to 150 kJ/mol. The main exceptions are phenyl alcohol (8) and allyl alcohol (11), with on average lower barriers, which can be attributed to mesomeric effects (+M). Similarly, methyl glycolate leads to higher barriers, which can be attributed to an −M mesomeric effect.

Conclusion

We investigated the first step of the stepwise dehydration of 13 alcohols within 8 different zeotypes using DFT calculations. Comparing the various initial and transition state energies, we found that differences in adsorption energies and barrier heights result mainly from differences in dispersive interactions between the alcohol and the zeotype, with larger alcohols also showing substantial repulsive interactions. These differences in dispersion interactions follow scaling rules such that the

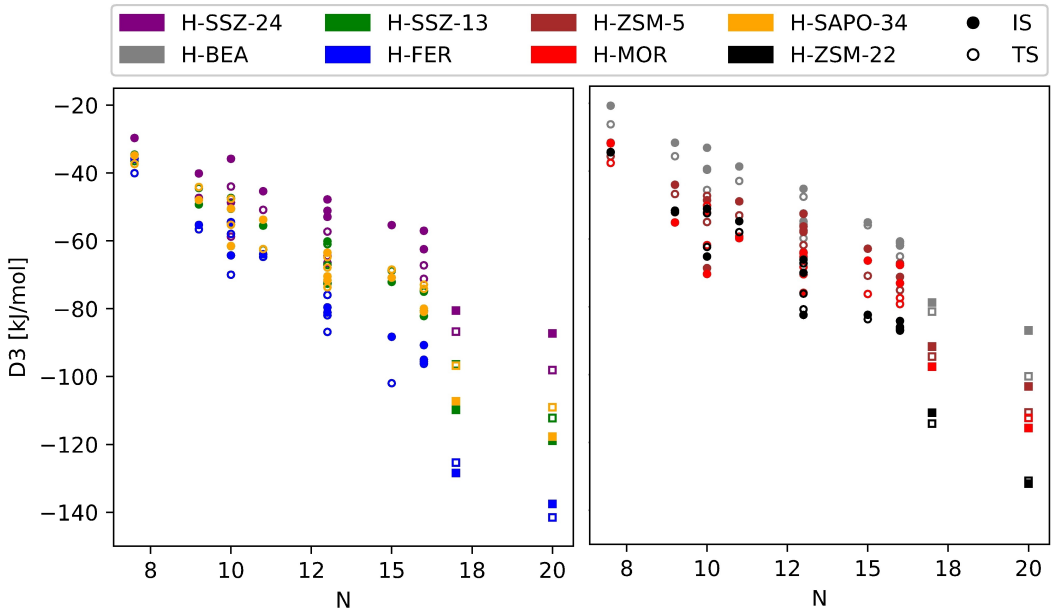

Figure 4. Dependence of the D3 (vdW) contribution to the energy of initial states (full symbols) and transition states (empty symbols) for all the studied zeolites and all the reactants from Scheme 1b. Reactants containing benzene are distinguished by squares. Energies are in kJ/mol, N stands for the total number of atoms of reactants including the Brønsted proton. The color code is the same as in Figure 2.

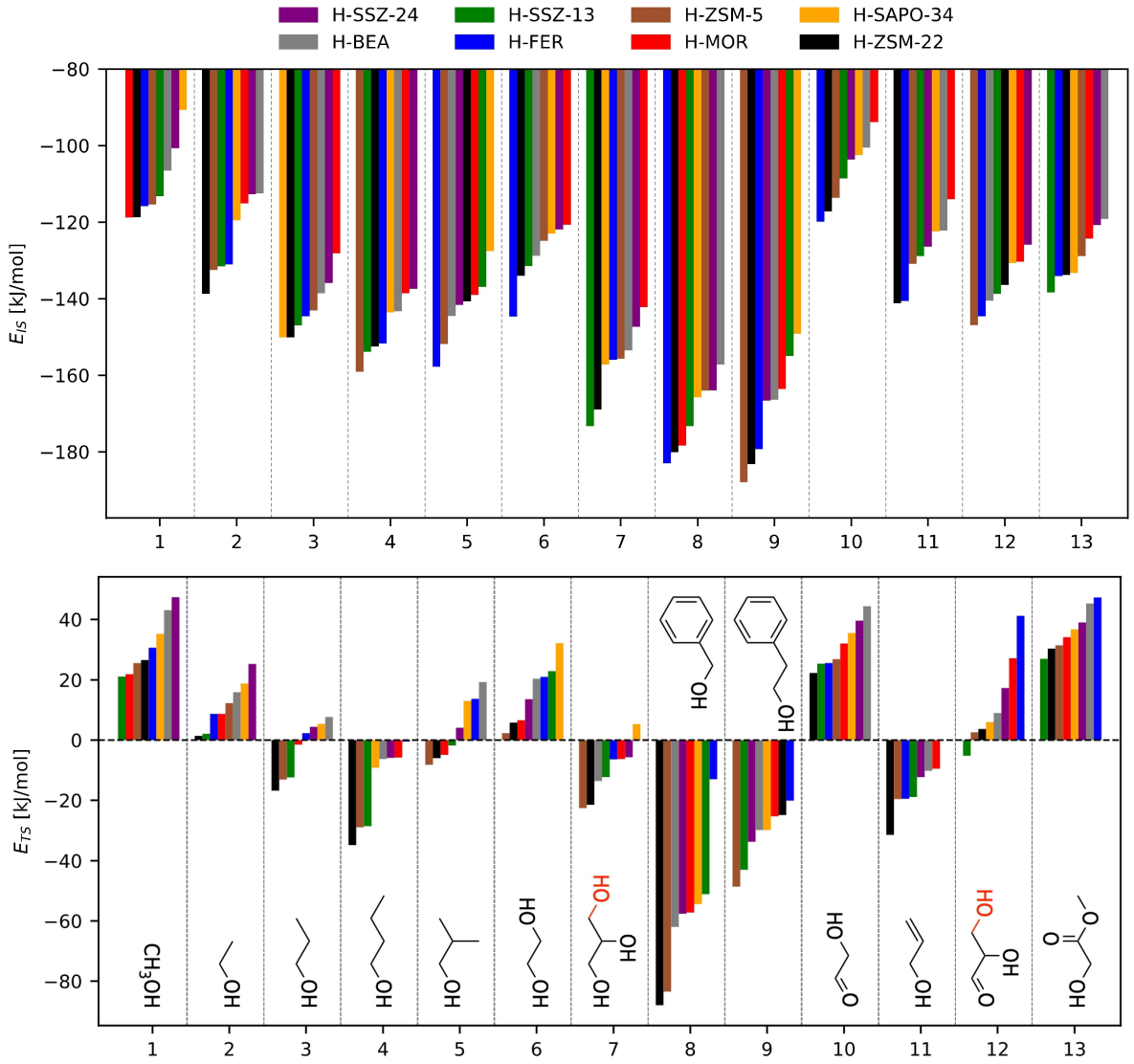

Figure 5. Reaction energies for initial states E_{IS} (top) and transition states E_{TS} (bottom) for all studied reactants and all studied zeolite frameworks. The numbering of the reactants is according to Scheme 1b and the molecules are additionally shown schematically at the bottom. The dehydrated OH groups are highlighted in red, where more than one option exists. The color scheme of the bar diagram is the same as in Figure 2. All energies are in kJ/mol and ZPVE corrected.

dispersion can in principle be estimated from the number of atoms of the adsorbate or transition state. Importantly, this scaling is different for the different frameworks investigated herein, with smaller pores having a steeper slope, that is, a stronger increase in dispersion interactions with the number of atoms in the corresponding alcohol. Our work shows that the interaction between a reactant and a zeotype is highly dependent on the nature of both, the reactant and zeotype, but can often be understood from a simple analysis of the chemical nature of the reactant. Our investigation is thus a first step towards the development of predictive rules to estimate adsorption energies and transition states within zeotypes without the need of costly computations.

Experimental Section

The computational setup is identical to that used in previous work.[19] Briefly, all DFT calculations were carried out using the Vienna Ab-initio Simulation Package (VASP)[52,53] in version 5.4.1 using the Atomic Simulation Environment (ASE).[54] The projector-augmented wave method (PAW) and the PBE functional[55,56] with D3 dispersion correction (zero damping),[57] PBE-D3, was used. All structures were fully optimized using a kinetic energy cut-off of 400 eV (800 eV for the optimization of lattice constants). Convergence criteria of 10^{-8} eV and 10^{-3} eV/Å were used for SCF cycles and geometry optimization, respectively. The optimized lattice constants are AFI (a = 13.886 Å, b = 13.886 Å, c = 8.606 Å), BEA (a = 12.700 Å, b = 12.700 Å, c = 26.600 Å), CHA (a = 13.625 Å, b = 13.625 Å, c = 15.067 Å), FER (a = 19.110 Å, b = 14.309 Å, c = 7.557 Å), MOR (a = 18.256 Å, b = 20.534 Å, c = 7.542 Å), and TON (a = 14.127 Å, b = 17.901 Å, c = 5.265 Å). In the case of AFI, FER, MOR and TON, we used a supercell consisting of two (AFI, FER, MOR) or three (TON) unit cells along their shortest lattice parameter to avoid

mutual interaction of acid sites. The acid site is modelled by substituting one Si with one Al (one P with a Si in the case of AlPO-34), introducing Brønsted acidity through a charge compensating proton. This way, the following zeolites were formed – H-SSZ-24 (AFI framework), H-BEA (BEA framework), H-SSZ-13 (CHA framework), H-FER (FER framework), H-MOR (MOR framework), H-SAPO-34 (CHA framework) and H-ZSM-22 (TON framework). The Si/Al ratios were thus 47/1 (H-SSZ-24 supercell), 63/1 (H-BEA), 35/1 (H-SSZ-13), 71/1 (H-FER supercell), 95/1 (H-MOR supercell), 71/1 (H-ZSM-22 supercell). For BEA, FER, MOR and TON frameworks, there are several places – tetrahedra sites (T-sites) – where the aluminium substitution can occur. For H-SSZ-13, H-SAPO-34 and H-BEA, we chose the same T-sites as in previous work of our group.[42–44] For other frameworks with multiple T-site, we used those found in literature. The T2 site for H-FER was used in earlier work of Sauer and co-workers,[45–47] the T4 site for H-MOR that is frequently used in calculations,[48–50] and the T1 site for H-ZSM-22 was used by Brogaard et al.[51] For each T-site, the proton can be located at each of the four connecting oxygen atoms – these together with further details and structures are given in SI. In case of H-ZSM-5 (MFI framework), the lattice parameters and chosen T- and O-site are the same as in previous works.[19,43] In the case of H-SSZ-13 and H-ZSM-5, the investigated O-sites were chosen based on the most stable site for the transition state of SMS-formation. For the other zeolites, the choice was based on the most stable site for adsorption of MeOH (see Table S2 in SI).

Transition states were located using the Automated Relaxed Potential Energy Surface Scans (ARPESS)[58] method and verified to have only one imaginary harmonic frequency corresponding to the transition vector of the reaction connecting initial and final states. Only part of the zeolites (the involved oxygen atom with the Brønsted proton and adjacent Si and Al atoms) together with the adsorbate were considered for the vibrational analysis. The vibrational frequencies were calculated using the harmonic oscillator approximation using a central finite-difference scheme with displacements of ± 0.01 Å. Out of different conformers for the same initial or transition state, only the most stable structures were considered in further analysis.

While the PBE-D3 functional employed herein has shown deficiencies concerning an accurate description of adsorption and transition state energies for zeolite catalysis,[59] we note that the trends from one zeolite material to the other, which is the key interest of this contribution, are well reproduced at this level of theory.[23]

Acknowledgements

The authors acknowledge support by the state of Baden-Württemberg through bwHPC (bwunicluster and JUSTUS, RV bw17D011). Financial support from the Helmholtz Association is also gratefully acknowledged. Open access funding enabled and organized by Projekt DEAL.

Conflict of Interest

The authors declare no conflict of interest.

Keywords: confinement · dehydration · density functional calculations · dispersion · zeolites

[1] J. Liang, Z. Liang, R. Zou, Y. Zhao, *Adv. Mater.* **2017**, *29*.
[2] V. Mouarrawis, R. Plessius, J. I. van der Vlugt, J. N. H. Reek, *Front. Chem.* **2018**, *6*, 623.
[3] M. Stöcker, *Microporous Mesoporous Mater.* **1999**, *29*, 3–48.
[4] U. Olsbye, S. Svelle, M. Bjorgen, P. Beato, T. V. Janssens, F. Joensen, S. Bordiga, K. P. Lillerud, *Angew. Chem. Int. Ed. Engl.* **2012**, *51*, 5810–5831.
[5] U. Olsbye, S. Svelle, K. P. Lillerud, Z. H. Wei, Y. Y. Chen, J. F. Li, J. G. Wang, W. B. Fan, *Chem. Soc. Rev.* **2015**, *44*, 7155–7176.
[6] I. Yarulina, A. D. Chowdhury, F. Meirer, B. M. Weckhuysen, J. Gascon, *Nat. Catal.* **2018**, *1*, 398–411.
[7] M. Dusselier, P. Van Wouwe, A. Dewaele, P. A. Jacobs, B. F. Sels, *Science* **2015**, *349*, 78–80.
[8] T. Ennaert, J. Van Aelst, J. Dijkmans, R. De Clercq, W. Schutyser, M. Dusselier, D. Verboekend, B. F. Sels, *Chem. Soc. Rev.* **2016**, *45*, 584–611.
[9] P. Rivalier, J. Duhamet, C. Moreau, R. Durand, *Catal. Today* **1995**, *24*, 165–171.
[10] K.-i. Shimizu, R. Uozumi, A. Satsuma, *Catal. Commun.* **2009**, *10*, 1849–1853.
[11] A. Corma, G. W. Huber, L. Sauvanaud, P. O'Connor, *J. Catal.* **2008**, *257*, 163–171.
[12] C.-J. Jia, Y. Liu, W. Schmidt, A.-H. Lu, F. Schüth, *J. Catal.* **2010**, *269*, 71–79.
[13] L. G. Possato, R. N. Diniz, T. Garetto, S. H. Pulcinelli, C. V. Santilli, L. Martins, *J. Catal.* **2013**, *300*, 102–112.
[14] B. Katryniok, S. Paul, V. Belliere-Baca, P. Rey, F. Dumeignil, *Green Chem.* **2010**, *12*, 2079–2098.
[15] K. Kongpatpanich, T. Nanok, B. Boekfa, M. Probst, J. Limtrakul, *Phys. Chem. Chem. Phys.* **2011**, *13*, 6462–6470.
[16] D. Lesthaeghe, V. Van Speybroeck, M. Waroquier, *Phys. Chem. Chem. Phys.* **2009**, *11*, 5222–5226.
[17] J. Van der Mynsbrugge, J. De Ridder, K. Hemelsoet, M. Waroquier, V. Van Speybroeck, *Chem. Eur. J.* **2013**, *19*, 11568–11576.
[18] R. Y. Brogaard, B. M. Weckhuysen, J. K. Nørskov, *J. Catal.* **2013**, *300*, 235–241.
[19] M. Fečík, P. N. Plessow, F. Studt, *J. Phys. Chem. C* **2018**, *122*, 23062–23067.
[20] M. Fečík, P. N. Plessow, F. Studt, *ACS Catal.* **2020**, *10*, 8916–8925.
[21] P. Ferri, C. Li, C. Paris, A. Vidal-Moya, M. Moliner, M. Boronat, A. Corma, *ACS Catal.* **2019**, *9*, 11542–11551.
[22] M. Boronat, A. Corma, *ACS Catal.* **2019**, *9*, 1539–1548.
[23] P. N. Plessow, F. Studt, *J. Phys. Chem. Lett.* **2020**, *11*, 4305–4310.
[24] C.-M. Wang, Y.-D. Wang, Z.-K. Xie, *Catal. Sci. Technol.* **2019**, *9*, 2245–2252.
[25] C. Liu, I. Tranca, R. A. van Santen, E. J. M. Hensen, E. A. Pidko, *J. Phys. Chem. C* **2017**, *121*, 23520–23530.
[26] C. M. Wang, R. Y. Brogaard, B. M. Weckhuysen, J. K. Norskov, F. Studt, *J. Phys. Chem. Lett.* **2014**, *5*, 1516–1521.
[27] A. Ghorbanpour, J. D. Rimer, L. C. Grabow, *Catal. Commun.* **2014**, *52*, 98–102.
[28] M. John, K. Alexopoulos, M.-F. Reyniers, G. B. Marin, *ACS Catal.* **2016**, *6*, 4081–4094.
[29] M. John, K. Alexopoulos, M.-F. Reyniers, G. B. Marin, *Catal. Sci. Technol.* **2017**, *7*, 2978–2997.
[30] A. A. Arvidsson, P. N. Plessow, F. Studt, A. Hellman, *J. Phys. Chem. C* **2020**, *124*, 14658–14663.
[31] A. J. Jones, E. Iglesia, *Angew. Chem. Int. Ed. Engl.* **2014**, *53*, 12177–12181.
[32] A. J. Hoffman, J. S. Bates, J. R. Di Iorio, S. V. Nystrom, C. T. Nimlos, R. Gounder, D. Hibbitts, *Angew. Chem. Int. Ed. Engl.* **2020**.
[33] H. Xin, X. Li, Y. Fang, X. Yi, W. Hu, Y. Chu, F. Zhang, A. Zheng, H. Zhang, X. Li, *J. Catal.* **2014**, *312*, 204–215.
[34] J. Meeprasert, S. Choomwattana, P. Pantu, J. Limtrakul, NSTI Nanotech, **2009**, pp. 288–291.
[35] M. DeLuca, P. Kravchenko, A. Hoffman, D. Hibbitts, *ACS Catal.* **2019**, *9*, 6444–6460.
[36] K. Bobuatong, M. Probst, J. Limtrakul, *J. Phys. Chem. C* **2010**, *114*, 21611–21617.
[37] K. Stuckenschneider, J. Merz, G. Schembecker, *J. Mol. Model.* **2013**, *19*, 5611–5624.
[38] F. Haase, J. Sauer, J. Hutter, *Chem. Phys. Lett.* **1997**, *266*, 397–402.
[39] M. N. Mazar, S. Al-Hashimi, A. Bhan, M. Cococcioni, *J. Phys. Chem. C* **2012**, *116*, 19385–19395.
[40] F. Haase, J. Sauer, *Microporous Mesoporous Mater.* **2000**, *35–36*, 379–385.
[41] K. Hemelsoet, A. Ghysels, D. Mores, K. De Wispelaere, V. Van Speybroeck, B. M. Weckhuysen, M. Waroquier, *Catal. Today* **2011**, *177*, 12–24.
[42] P. N. Plessow, F. Studt, *ACS Catal.* **2017**, *7*, 7987–7994.

[43] P. N. Plessow, F. Studt, *Catal. Lett.* **2018**, *148*, 1246–1253.
[44] T. J. Goncalves, U. Arnold, P. N. Plessow, F. Studt, *ACS Catal.* **2017**, *7*, 3615–3621.
[45] C. Tuma, J. Sauer, *Phys. Chem. Chem. Phys.* **2006**, *8*, 3955–3965.
[46] V. Nieminen, M. Sierka, D. Murzin, J. Sauer, *J. Catal.* **2005**, *231*, 393–404.
[47] C. Tuma, J. Sauer, *Angew. Chem. Int. Ed. Engl.* **2005**, *44*, 4769–4771.
[48] M. Brändle, J. Sauer, *J. Am. Chem. Soc.* **1998**, *120*, 1556–1570.
[49] X. Rozanska, R. A. van Santen, T. Demuth, F. Hutschka, J. Hafner, *J. Phys. Chem. B* **2003**, *107*, 1309–1315.
[50] I. Stich, J. D. Gale, K. Terakura, M. C. Payne, *Chem. Phys. Lett.* **1998**, *283*, 402–408.
[51] R. Y. Brogaard, R. Henry, Y. Schuurman, A. J. Medford, P. G. Moses, P. Beato, S. Svelle, J. K. Nørskov, U. Olsbye, *J. Catal.* **2014**, *314*, 159–169.
[52] G. Kresse, J. Furthmüller, *Phys. Rev. B* **1996**, *54*, 11169–11186.
[53] G. Kresse, D. Joubert, *Phys. Rev. B* **1999**, *59*, 1758–1775.
[54] A. H. Larsen, J. J. Mortensen, J. Blomqvist, I. E. Castelli, R. Christensen, M. Dulak, J. Friis, M. N. Groves, B. Hammer, C. Hargus, E. D. Hermes, P. C. Jennings, P. Bjerre Jensen, J. Kermode, J. R. Kitchin, E. Leonhard Kolsbjerg, J. Kubal, K. Kaasbjerg, S. Lysgaard, J. Bergmann Maronsson, T. Maxson, T. Olsen, L. Pastewka, A. Peterson, C. Rostgaard, J. Schiotz, O. Schutt, M. Strange, K. S. Thygesen, T. Vegge, L. Vilhelmsen, M. Walter, Z. Zeng, K. W. Jacobsen, *J. Phys. Condens. Matter* **2017**, *29*, 273002.
[55] J. P. Perdew, K. Burke, M. Ernzerhof, *Phys. Rev. Lett.* **1996**, *77*, 3865–3868.
[56] J. P. Perdew, K. Burke, M. Ernzerhof, *Phys. Rev. Lett.* **1997**, *78*, 1396–1396.
[57] S. Grimme, J. Antony, S. Ehrlich, H. Krieg, *J. Chem. Phys.* **2010**, *132*, 154104.
[58] P. N. Plessow, *J. Chem. Theory Comput.* **2018**, *14*, 981–990.
[59] T. J. Goncalves, P. N. Plessow, F. Studt, *ChemCatChem* **2019**, *11*, 4368–4376.

Manuscript received: January 4, 2021
Revised manuscript received: February 25, 2021
Version of record online: ■■, ■■■

FULL PAPERS

Just the type! The influence of the confinement imposed by eight different zeotypes on the formation of the alkoxides of 13 primary alcohols is studied using dispersion corrected density functional theory calculations with the PBE-D3 functional. Adsorption energies of the alcohols are computed along with barriers for formation of the alkoxides, which is the first step of the stepwise dehydration mechanism.

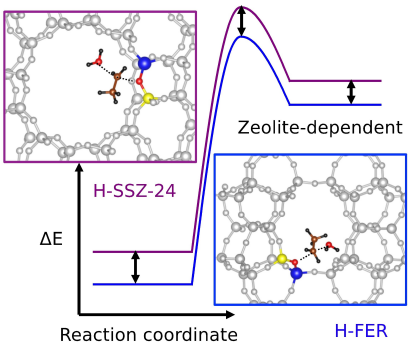

M. Fečík, Dr. P. N. Plessow, Prof. F. Studt**

1 – 9

Influence of Confinement on Barriers for Alkoxide Formation in Acidic Zeolites